CrossMark

Creep behavior and microstructure of a 9Cr–3Co–3W martensitic steel

A. Fedoseeva[1,*], N. Dudova[1], and R. Kaibyshev[1]

[1] Belgorod State University, Pobeda 85, 308015 Belgorod, Russia

ABSTRACT

Microstructure evolution under long-term aging and creep was studied in a 9wt%Cr–3wt%Co–3wt%W martensitic steel at a temperature of 650 °C and stress ranging from 100 to 220 MPa with a step of 20 MPa. This steel exhibited creep strength breakdown at an applied stress of 160 MPa and a rupture time of 1703 h. However, this creep strength breakdown did not coincide with the transition from short-term creep conditions to long-term creep, because deviation from the Monkman–Grant relationship occurs at a minimal strain rate of $\sim 3 \times 10^{-6}\,\text{h}^{-1}$, and the acceleration of the creep rate by strain, $d\ln \dot{\varepsilon}_r/d\varepsilon$, in the acceleration region at applied stresses of 120 and 100 MPa significantly differs from the acceleration at greater applied stresses. The transition from short-term creep to long-term creep correlates with the strain-induced coarsening of the $M_{23}C_6$ carbides and the Laves phase particles, which leads to dissolution of the fine particles and the growth of coarse particles of these phases at the lath boundaries. With a decrease in the applied stress, the overall Zener drag force exerted by the boundary particles decreases below the critical value of 0.12 MPa, and the tempered martensitic lath structure transforms to a subgrain structure.

Introduction

Heat-resistant steels with 9–12%Cr are widely used as structural materials for boilers, steam main tubes, and turbines of fossil power plants to increase thermal efficiency [1, 2]. The tempered martensite lath structure (TMLS) consisting of prior austenite grains (PAG), packets, blocks, and laths and containing a high density of separate dislocations and a dispersion of secondary-phase particles evolves after heat treatment [1–5]. The superior creep resistance of these steels is attributed to the stability of the TMLS under long-term aging and creep provided by the $M_{23}C_6$-type carbides and M(C,N) carbonitrides precipitated at boundaries and within the ferritic matrix, respectively, during tempering, and the boundary Laves phase particles precipitated during creep [1, 2, 4–12]. The main limiting factor for the increase in the service temperature of 9–12%Cr steels is the creep strength breakdown accompanied by premature fracture at a low stress due to the evolution of a dispersion of secondary phases and

Address correspondence to E-mail: fedoseeva@bsu.edu.ru

the transformation of the TMLS to a subgrain structure [7, 13–15].

Under creep the lattice mobile dislocations can interact with intrinsic dislocations of lath boundaries, which leads to the mutual annihilation of the dislocations with the opposite sign [5, 6, 16–19]. Dislocation climb is a necessary condition for the occurrence of this reaction, because annihilation events take place by climb of two dislocations with the opposite signs through critical annihilation distance [17–20]. Lath boundaries play a role of sinks for lattice dislocations [19]. Concurrently, climb of dislocations in the lath boundaries leads to the transformation of these boundaries, which are, in fact, irregular dislocation networks, to subboundaries. These processes are termed as the knitting reactions and relive the internal long-range strain fields [6, 7, 16–23]. Next, the migration of the lath boundaries leads to the formation of a well-defined subgrain structure instead of the TMLS [5, 7–9, 12]. Kostka et al. showed that a dispersion of carbides plays a key role in impeding the knitting reaction and hindering lath boundary migration by exerting Zener drag force [6, 22]. M(C,N) (where M—V or Nb) carbonitrides and boundary $M_{23}C_6$ carbides are highly effective in pinning the mobile lattice dislocations and preventing their interaction with sessile dislocations, which compose the lath boundaries [6, 7]. Boundary $M_{23}C_6$ carbides and Laves phase particles that exert a high Zener drag force hinder subgrain coarsening [7, 9–11]. Matrix M(C,N) carbonitrides provide a minor contribution to the overall pinning pressure [7, 9–11].

The dispersion of secondary-phase particles withstands short-term creep [1, 4–15]. Coarsening of the boundary $M_{23}C_6$ carbides and the Laves phase particles through Ostwald ripening and the replacement of nanoscale M(C,N) carbonitride particles by Z-phase (CrVN) micron particles [1, 7, 9–12, 24–29] diminish their efficiency as pinning agents and facilitate the knitting reaction and subboundary migration. The enhanced creep strength could be achieved through a pronounced stability of the dispersion of the secondary phase under long-term creep. An effective way to attain this goal is to slow down the diffusion using substitutional additives, such as Co and W, that decrease the rate of dislocation climb [1, 5, 7, 9, 30–32]. These additions significantly hinder the coarsening of $M_{23}C_6$ carbides and Laves

phase particles, and the replacement of M(C,N) carbonitrides by Z-phase particles, which results in the superior creep resistance of martensitic steels [9, 13, 31, 32]. The efficiency of W as an alloying element in hindering diffusion is greater than that of Co [1]. However, no depletion of Co from the ferritic matrix occurs under creep conditions, whereas W and Mo have limited solubility within ferrite, and their excessive content is depleted from the solid solution leading to the precipitation of W/Mo-rich particles, such as Laves phase particles $Fe_2(W,Mo)$ or M_6C carbides under creep conditions [1, 7, 9–11, 31, 33–42]. This depletion does not occur in 9%Cr steel containing no or <1 wt% W [1, 7, 42]. Depletion of the solid solution by these elements induces a significant coarsening of the $M_{23}C_6$ carbides and the Laves phase particles [1, 4, 7–11] that greatly deteriorates the creep resistance and correlates with the creep strength breakdown and the replacement of TMLS by well-defined subgrain structure [1, 4, 7, 9–15, 26, 29, 42].

It is worth noting that only a few limited examinations of the W-effect on creep behavior have been carried out for Co-free high-chromium martensitic steels [32–35, 42]. The aim of the present work is to examine the effect of a 1 wt% W addition on the creep behavior and microstructural evolution subjected to long-term aging and creep. To achieve this goal, a 0.1C–0.05N–9Cr–3Co–3W–0.5Mo–0.2V–0.05Nb steel is examined. The experimental data obtained are compared with data for a P92 steel [10, 43].

Materials and methods

A steel, which is denoted here as 9Cr3W, with the chemical composition (in wt%) Fe (bal.)–0.12C–9.5Cr–3.2Co–3.1W–0.45Mo–0.06Si–0.2Mn–0.2V–0.06Nb–0.05N–0.005B, was prepared by air melting 20 kg ingots. Square bars with a 13×13 mm^2 cross section were cast and hot forged by the Central Research Institute for Machine-Building Technology, Moscow, Russia. This steel was solution treated at 1050 °C for 30 min, cooled in air, and subsequently tempered at 750 °C for 3 h. Flat specimens with a gage length of 25 mm and a cross section of 7×3 mm^2, and cylindrical specimens with gage length of 100 mm and a 10 mm diameter were crept until rupture at 650 °C under an applied stress ranging from 100 to 220 MPa with a step of 20 MPa.

The structural characterization was carried out using a transmission electron microscope JEOL-2100 (TEM) with an INCA energy-dispersive X-ray spectrometer (EDS) and a Quanta 600FEG scanning electron microscope (SEM) on ruptured creep specimens. Identification of the precipitates was performed based on combination of EDS composition measurements of the metallic elements using the manufacturer's library of internal reference standards and indexing of the electron diffraction patterns using TEM. The subgrain sizes were evaluated on TEM micrographs using the linear intercept method including all clearly visible subboundaries. The dislocation densities in the grain/subgrain interiors were estimated as a number of intersections of individual dislocations with upper/down foil surfaces per unit area on at least six arbitrarily selected typical TEM images for each data point [44]. The dislocation observation was carried out under multiple-beam conditions with large excitation vectors for several diffracted planes for each TEM image. M_6C carbides and Laves phase particles were separated from each other using TEM EDS composition measurements and using the particle-size distribution. The volume fractions of the precipitated phases were calculated using the Thermo-Calc software with the TCFE6 database for the following steel composition (in wt%): Fe–0.1C–9.4Cr–0.5Mo–3.0W–3.0Co–0.2V–0.05Nb–0.05N–0.005B. The following phases were selected independently for calculation: BCC, FCC, $M_{23}C_6$ carbide, Laves phase ($Fe_2(W,Mo)$) (C14).

Experimental results

Initial structure

The structural characteristics of the TMLS of the 9Cr3W steel after normalizing and tempering at 750 °C are summarized in Table 1. The microstructure and the distributions of the secondary-phase particles were described in a recent work [45] in detail. Major portions of the $M_{23}C_6$ carbides were located on the high-angle boundaries of the PAGs/packets/blocks, whereas the $M_{23}C_6$ carbides along the lath boundaries were rarely observed (Fig. 1a, c). In addition, the W-rich M_6C carbides (Fe_3W_3C) and the Laves phase (Fe_2W) particles were found at the boundaries (Fig. 1d, e). The dimensions of the fine-boundary $M_{23}C_6$ carbides and the Laves phase particles were nearly the same (<100 nm) (Table 1), whereas the average size of the M_6C carbides was ∼350 nm (Fig. 1d, e). As a result, a wide size distribution of W-rich particles was observed (Fig. 1b). M(C,N) carbonitrides were uniformly distributed within the martensitic laths (Fig. 1c). Two-phase separation of these carbonitrides [1, 8, 45] into V-rich M(C,N), with a plate-like shape and a mean longitudinal size of 20 nm, and Nb-rich M(C,N) carbonitrides, with a round shape and an average size of ∼40 nm, took place.

Creep behavior

Figure 2 shows the creep rupture data of the steels at a temperature of 650 °C. The variation in the rupture

Table 1 Evolution of structural parameters after tempering at $T = 750$ °C, aging at $T = 650$ °C, and creep testing at $T = 650$ °C when subject to different stresses

| Structural parameters	Initial state	Aging/creep										
		220 (50 h)		200 (207 h)		180 (454 h)		160 (1703 h)		140 (3489)		100 (15,998 h)	
		Grip	Gage	Grip	Gage	Grip	Gage	Grip	Gage	Grip	Gage	Grip	Gage
D_{PAG} (µm)	20	20	20	20	20	20	20	20	20	20	20	20	20
D_{laths} (µm)	0.38	0.43	0.41	0.43	0.51	0.43	0.57	0.40	0.57	0.42	0.6	0.42	0.78
$D_{subgrains}$ (µm)	–	–	0.45	–	0.58	–	0.62	0.30	0.68	0.35	0.7	0.41	0,76
Dislocation density, $\times 10^{14}$ m^{-2}	2.6	1.8	1.3	1.8	1.2	1.8	1.1	1.8	1.0	1.1	1.0	1.0	0.46
Mean size of $M_{23}C_6$ (nm)	90	86	88	86	97	98	100	93	101	85	113	133	236
Mean size of Laves phase (nm)	90	90	93	95	110	105	108	110	113	113	130	230	532
Mean size of VX (nm)	20	50	48	50	50	50	58	49	52	50	54	48	82
Mean size of CrVN (nm)	–	–	–	–	–	–	–	–	–	–	–	–	50
Mean size of NbX (nm)	40	70	70	70	70	70	70	70	70	70	70	70	70
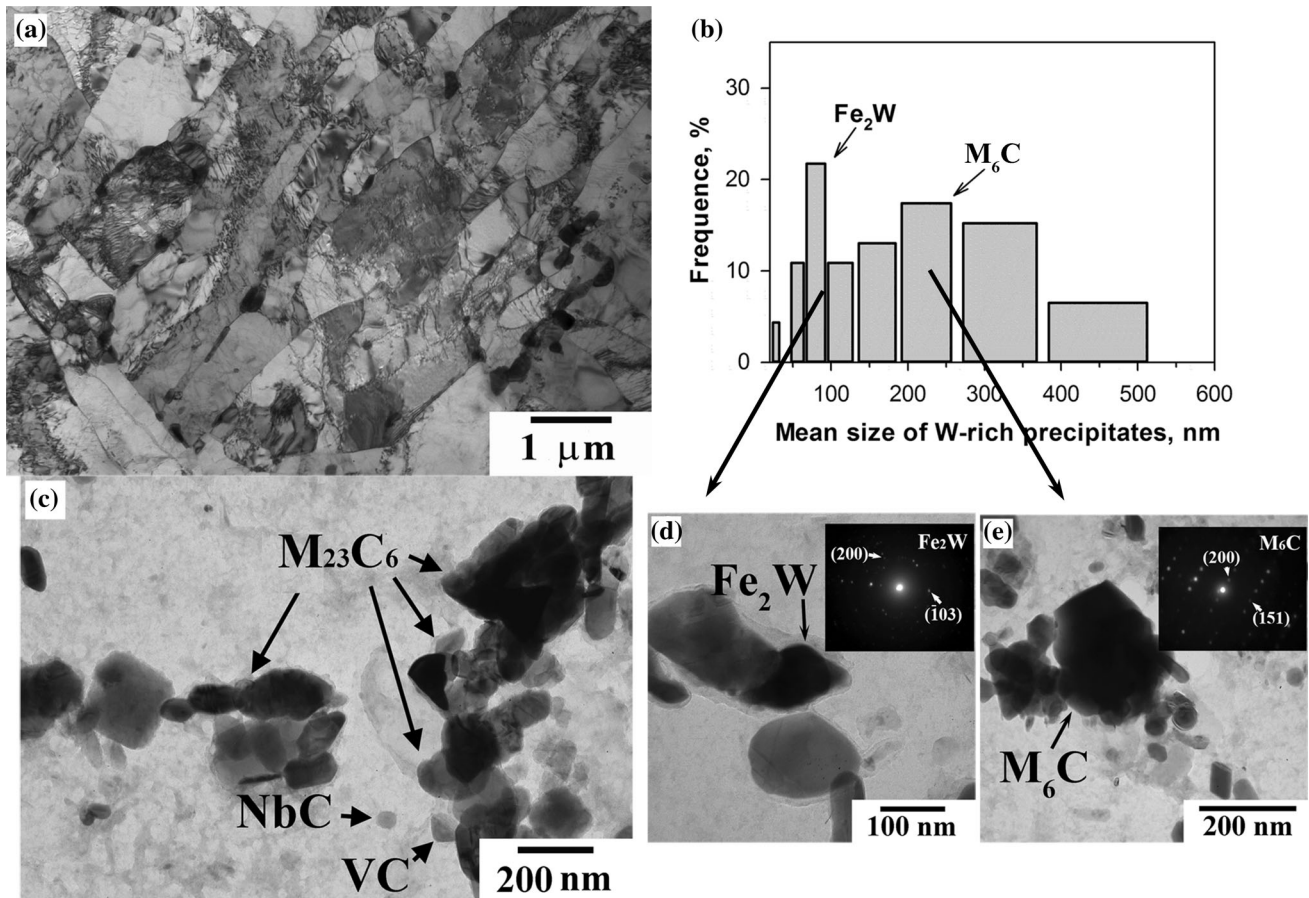
Figure 1 Typical microstructure of the 9Cr3W steel after normalizing and tempering at 750 °C: TEM of foils (**a**) and replicas (**c**–**e**) and the size distribution of the W-rich precipitates (**b**).
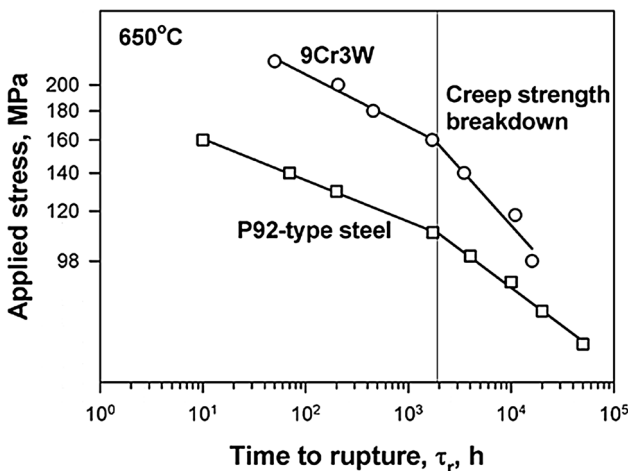

Figure 2 Time to rupture versus stress curve shows the creep strength breakdown for the 9Cr3W and P92 steels [36].

time with an applied stress for a P92-type steel [43] was also presented for comparison. The 3%Co and 3%W additions significantly increased the creep

strength under the high applied stresses. Approximately 170-, 45-, and 40-fold differences in the creep rupture time were observed between the P92 [43] and the 9Cr3W steels at applied stresses of 160, 140, and 100 MPa, respectively. Under the low applied stress (less 140 MPa), the effect of the Co and W additives on the creep strength tends to diminish. Well-defined creep strength breakdown [1, 7, 13–15, 43] was observed at ~2000 h of creep for both steels. The 3%Co and 3%W additives increased the level of an applied stress, at which the creep strength breakdown was observed, from 110 to 160 MPa. It is worth noting that the high B and Mo-free 9Cr–3Co–3W steels developed at the National Institute for Materials Science (NIMS) exhibited creep strength breakdown at applied stress of 120 MPa with corresponding rupture time of ~10^4 h (MARBN10 steel with B content of 0.01 wt%) or no the creep strength breakdown appeared up to rupture times of ~4×10^4 h (MARBN12 steel with B content of

0.012 wt%) [46]. Superior creep strength of these steels was attributed to a strong effect of such elements as B, N, Mn, Ni on a dispersion of boundary $M_{23}C_6$ carbides [46–48].

The creep rate versus time and strain curves at 650 °C for the different nominal stresses (100–200 MPa) are shown in Fig. 3a, b. The creep behavior was typical for heat-resistant martensitic steels containing dispersed particles. The minimum creep rate decreased from approximately 10^{-7} to 10^{-10} s^{-1} with a decrease in the applied stress from 220 to 100 MPa. There was a linear dependence between the minimum creep rate and the applied stress (Fig. 3c). The experimental data obey a power law relationship throughout the whole range of the applied stress of the usual form [1, 7, 49, 50]:

$$\dot{\varepsilon}_{min} = A \times \sigma^n \exp\left(\frac{-Q}{RT}\right), \tag{1}$$

where $\dot{\varepsilon}_{min}$ is the minimum creep rate, σ is the applied stress, Q is the activation energy for a plastic deformation, R is the gas constant, T is the absolute temperature, A is a constant, and n is the "apparent" stress exponent. This plot provides the best linear fit with a regression coefficient of 0.98 for $n = 9$ for the whole applied stress interval. This n value at all tested stress regimes remains constant. The steady-state stage of the 9Cr3 W steel was controlled using the same process for short- and long-term regions at a creep rate ranging from 10^{-6} to 10^{-10} s^{-1}. This clearly indicates that there is no creep strength breakdown during the steady-state stage of creep of the 9Cr3 W

steel [7, 13]. Abe showed [13] that the time to rupture correlates with the minimum creep rate, $\dot{\varepsilon}_{min}$, in a Co-free 9% Cr steel (P91). However, no such correlation was observed in 9%Cr steels containing ≥2 wt% W [7, 21, 23]. At applied stress of ≥100 MPa, the creep strength breakdown was not accompanied by a decrease in the stress exponent, n, as in a P91 steel [13].

In contrast with the dependencies of the applied stress versus the rupture time (Fig. 2), the distinct inflection point for the transition from a short-term region to a long-term one by shapes of aforementioned curves was observed at an applied stress of 120 MPa. The elongation-to-failure increases with a decrease in the applied stresses to 140 MPa and then decreases further at 120 and 100 MPa (Fig. 4a). The 3- and 5-fold decreases in the ductility take place at 120 and 100 MPa, respectively, compared with the elongation-to-failure at an applied stress of 140 MPa. The off-set strain, ε_{min}, which is the strain where the minimum creep rate is attained, exhibits linear dependence on the applied stress (Fig. 4b). The onset of acceleration creep occurs when the creep strain achieves 1.5–3% and less than 1% at high stresses and low stresses, respectively (Fig. 4b). The decrease in the off-set strain with a decrease in the applied stress supports the fact that the deformation in the transient creep stage becomes localized at low stresses [13]. Effect of an applied stress on the contribution to creep deformation incurred by the transient creep strain, ε_T, creep strain accumulation at the minimum creep rate ($\varepsilon_{min} \times t_r$, where t_r is rupture time), and tertiary creep
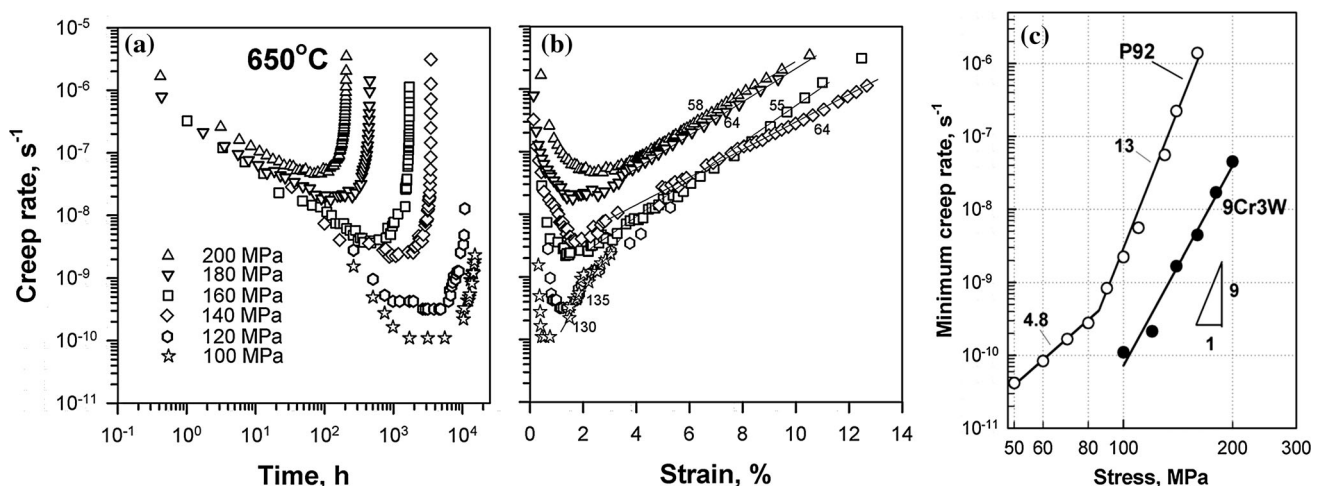

Figure 3 Creep rate versus time (**a**) and creep rate versus strain (**b**) curves at 650 °C and different stresses from 100 to 200 MPa, the stress dependence of the minimum creep rate (**c**) of the steel studied in comparison with data for P92 steel [36].
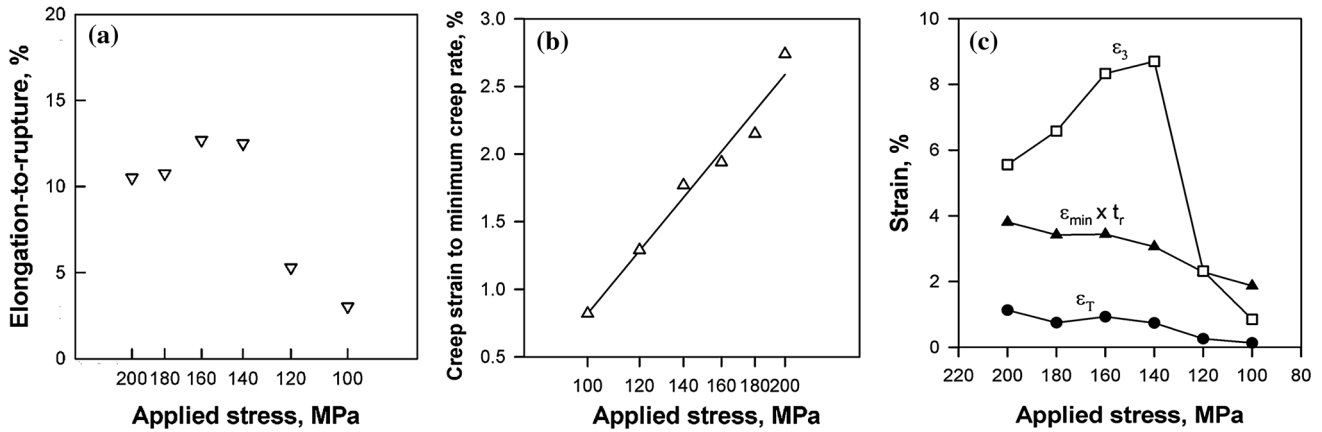
Figure 4 Effect of applied stress on the elongation-to-rupture (**a**), the off-set strain at which the minimum creep rate was attained for the 9Cr3W steel (**b**), and the contribution to creep deformation incurred by the transient creep strain, ε_T, creep strain accumulation at the minimum creep rate, $\varepsilon_{min} \times t_r$, and tertiary creep strain, ε_3 (**c**).

strain, ε_3, [13, 33, 34] is shown schematically in Fig. 4c. It is seen that at applied stress ≥ 140 MPa, the values of all these strain ranges (ε_T, ($\varepsilon_{min} \times t_r$) and ε_3) slightly depend on the applied stress. A decrease in the applied stress from 140 to 120 MPa leads to the 3- and 4-fold decreases in the ε_T and ε_3 values, respectively, and a -22% decrease in the $\varepsilon_{min} \times t_r$ value.

It was recently shown that creep strength breakdown is a tertiary creep phenomenon [7, 13]. The Monkman–Grant relationship [51] relating the rupture time, τ_r, to the minimum or steady-state creep rate is described as:

$$\tau_r = (c'/\dot{\varepsilon}_{min})^{m'}, \tag{2}$$

where c' and m' are constants. This relationship is used for the prediction of creep life of heat-resistant steels [1, 13]. Analysis of Eq. (2) for the studied steel (Fig. 5) shows that this approach is suitable for describing the relation of rupture time with the off-set strain rate, $\dot{\varepsilon}_{min}$. For short-term conditions, which corresponds to a τ_r less than approximately 3500 h, τ_r is inversely proportional to $\dot{\varepsilon}_{min}$ (Fig. 5) at $m' = 1$. The constant c' is 3.0×10^{-2}. For long-term conditions, which corresponded to a τ_r greater than approximately 3500 h, the relationship between τ_r and $\dot{\varepsilon}_{min}$ deviates downward. The transition from short-term creep to long-term creep appears as the deviation from the linear dependence described by Eq. (2), which indicates $m' < 1$ [13], at an applied stress ≤ 120 MPa. In the 9Cr steels containing ≥ 2 wt% W, the creep strength breakdown is attributed to the strong acceleration of tertiary creep [7].
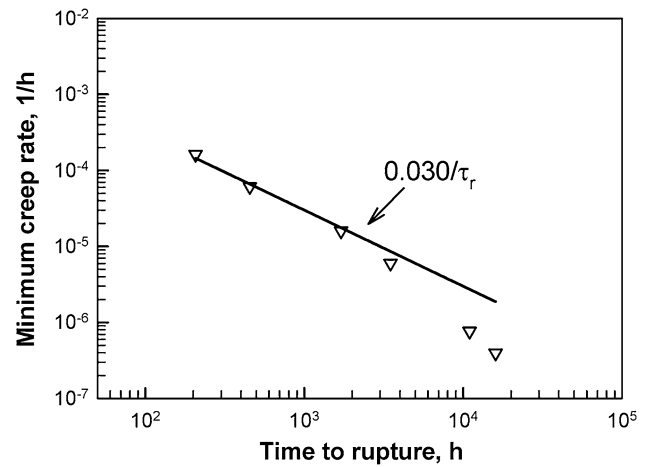

Figure 5 Minimum creep rate as a function of time to rupture for the 9Cr3W steel.

Figure 6a demonstrates the change in the slope of the curves shown in Fig. 3b in creep acceleration region ($d\ln \dot{\varepsilon}_r/d\varepsilon$) estimated using the method suggested in [13], where $\dot{\varepsilon}_r$ and ε are the creep rate and the creep strain, respectively, at a time t. Value of $d\ln \dot{\varepsilon}_r/d\varepsilon$ increases with a decrease in the stress. The dependence of the strain rate on the strain in the acceleration region is described as [13]:

$$\dot{\varepsilon} = \dot{\varepsilon}_0 \exp(n\varepsilon) \exp(m\varepsilon) \exp(d\varepsilon) \exp(i\varepsilon) \tag{3}$$

$$d\ln\dot{\varepsilon}/d\varepsilon = n + m + d + i, \tag{4}$$

where $\dot{\varepsilon}_0$ is the initial creep rate, n is the stress exponent from Eq. (1) and is 9 for the whole applied stress interval for the 9Cr3W steel, m is the microstructure degradation parameter, d is damage parameter due to the creep voids, and i describes the
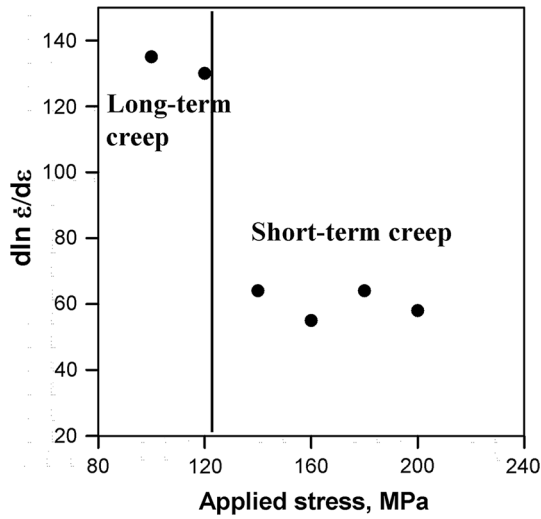
Figure 6 Stress dependence of dln $\dot{\varepsilon}_r/d\varepsilon$ in the acceleration creep stage of the 9Cr3W steel.

localized creep deformation [13]. As suggested in [13], parameter d is neglected because there is no evidence for cavitation in the 9Cr3W steel. Therefore, dln $\dot{\varepsilon}_r/d\varepsilon$ results from the parameters n, m, and i. At high stresses of 200–140 MPa, the dln $\dot{\varepsilon}_r/d\varepsilon$ ranges from 45 to 60. Therefore, when subject to stresses ranging from 200 to 140 MPa, the microstructural evolution has an insignificant effect on the tertiary creep behavior [13]. Conversely, at an applied stress of <120 MPa, dln $\dot{\varepsilon}_r/d\varepsilon$ increases to approximately 130 indicating a key role of microstructural changes in the softening of the 9Cr3W steel during tertiary creep. Therefore, creep strength breakdown does not coincide with the deviation from the linear dependence of the Monkman–Grant relationship that occurred at applied stresses less than 120 MPa, and during tertiary creep, the acceleration of the creep rate by the strain, dln $\dot{\varepsilon}_r/d\varepsilon$, distinctly differs from that at greater applied stresses. Therefore, the present data are unambiguously indicative that the creep strength breakdown is a tertiary creep phenomenon [1, 7, 13], is distinguished by a strong decrease in the ε_3 value, and increased the rate of acceleration of tertiary creep characterized a high dln $\dot{\varepsilon}_r/d\varepsilon$ value at an applied stress ≤120 MPa.

Hardness behavior

In the grip portion of the creep specimens, the hardness remained virtually unchanged up to ~10^3 h and dropped at approximately 2000 h
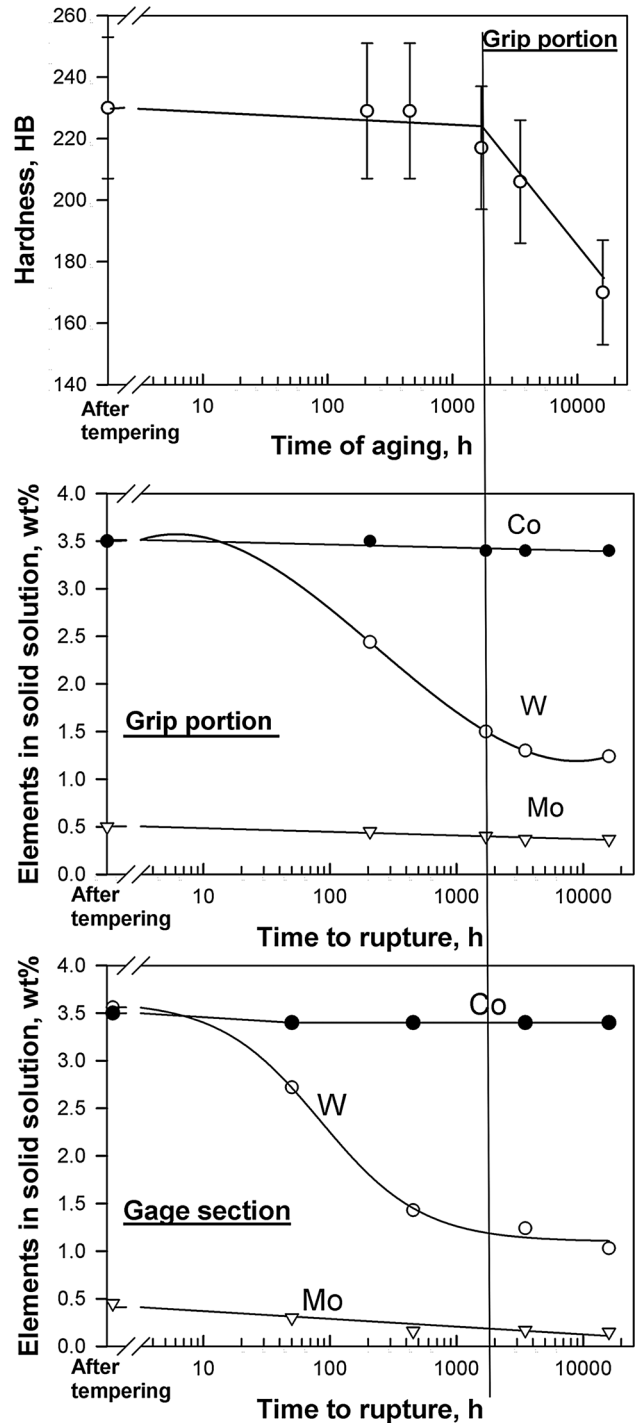

Figure 7 Hardness decrease in the grip portion (**a**) was accompanied by the depletion of W from the solid solution in the grip (**b**) and the gage sections (**c**).

(Fig. 7a). This effect of long-term aging on hardness correlates with a breakdown in the creep strength curve (Fig. 2) and a depletion of the major portion of the W from the solid solution (Fig. 7b, c). It is worth
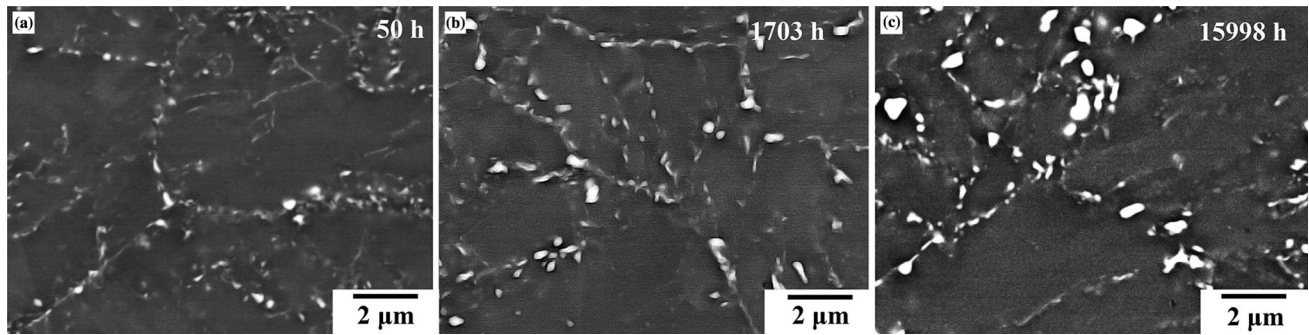
Figure 8 Microstructure of the 9Cr3W steel in the grip portion after long-term aging at $T = 650\,°C$ for 50 (**a**), 1703 (**b**), and 15,998 h (**c**).

noting that the Co content in the solid solution is independent of the exposure time for any creep conditions and under long-term aging. Strong strain-induced depletion of W and Mo from the solid solution took place at an exposure time of less than 10^3 h (Fig. 7c). Thermodynamic equilibrium of the elemental content in the solid solution was attained in specimens aged for 2000 h. Therefore, the depletion of W and Mo was complete in the short-term creep region. It is worth noting that, at rupture times of ≥2000 h, the $Mo_{eq} = \Sigma(Mo + 0.5W)$ in the present steel and the 3%Co P92-type steel [7] became the same. Therefore, an increased W content provides additional solutes of this element in solid solution for only a limited time.

Microstructures after long-term aging

Effect of long-term aging on microstructure and a dispersion of secondary phases was examined in the grip portion of samples, in which the thermally aged condition without stress occurred, compared to the gage section. No significant changes in the TMLS took place under long-term aging (Fig. 8; Table 1) even after 1.6×10^4 h. The lath thickness remained nearly unchanged, and the dislocation density decreased by a factor of more than 2 after 3.5×10^3 h (Figs. 8, 9a; Table 1). Concurrently, minor portions of the laths transformed to subgrains with approximately round shapes. However, the average size of subgrains and the lath thickness were nearly the same (Table 1). Therefore, this transformation occurred due to the subdivision of some laths by the transverse boundaries and was not accompanied by subgrain coarsening.

Additional precipitation of the Laves phase particles at the PAG boundaries occurred during short-term aging. Precipitation of fine particles at the lath boundaries continuously appeared (Fig. 8). As a result, the lath boundaries became decorated by fine Laves phase particles even after 1.6×10^4 h. A strong acceleration of the coarsening took place after the depletion of a major part of W from the solid solution, which led to the formation of the chains of coarse Laves phase particles along the boundaries of the PAGs (Figs. 7, 8). Full replacement of M_6C carbides, which is transition phase, by the Laves phase, which is the thermodynamical equilibrium phase [45, 52], occurred after 50 h of aging.

The mean size of the $M_{23}C_6$ carbides remained nearly unchanged during long-term aging up to $\sim 3.5 \times 10^3$ h, because insignificant additional precipitation of these carbides occurred (Fig. 9b; Table 1). As it was shown by O. Prat et al. [29], the $M_{23}C_6$ carbides can reach their equilibrium volume fraction for 300 h of aging in the 12%Cr steels with a high content of W and Co. Additional precipitation of $M_{23}C_6$ carbides was detected during creep in the 3 wt% Co-modified 9/12%Cr steels containing ≥3wt % W. A +20% increase in the average dimension was observed after up to $\sim 1.6 \times 10^4$ h due to the coarsening of these carbides located at the boundaries of the PAGs/packets/blocks. The average sizes of the $M_{23}C_6$ carbides and the Laves phase particles in the present steel after long-term aging for 3×10^3 h were smaller compared to a 9Cr–3Co–3W–0.014B steel [48].

Furthermore, 50 h of aging resulted in a +150% increase in the size of V-rich M(C,N) carbonitrides and a +75% increase in the dimensions of the Nb-rich particles (Fig. 9b; Table 1). No remarkable effect of further long-term aging on the distribution of M(C,N) carbonitrides was found. It is worth noting that an insignificant increase in the volume fraction of V-rich M(C,N) carbonitrides occurred. All V-rich M(C,N)

examined contained ≤20 at.% Cr, and therefore, no evidence for the formation of a Z-phase was observed [24].

Short-term creep microstructures

When subject to short-term creep conditions, the lath structure is nearly retained because the difference in the lath thickness and the dislocation density between the grip and gage lengths was less than 42% (Table 1). A minor part of laths transformed to sub-grains in a manner similar to long-term aging

Figure 9 Mean size of the subgrain/lath and dislocation spacing (**a**) and the mean size of particles in the grip (**b**) and gage sections (**c**) of specimens as a function of time in the 9Cr3W steel during creep tests at 650 °C subject to stresses of 100–220 MPa.

of $\geq 3.5 \times 10^3$ h. An insignificant increase in the lath thickness occurred (Fig. 9a; Table 1).

A major portion of the W and Mo that was depleted from solid solution was consumed for the formation of new Laves phase particles. A major portion of the Laves phase particles precipitated at the lath boundaries. The precipitation of this phase at the boundaries of the PAGs/packets/blocks also took place (Fig. 10a, b). As a result, a strong increase in the density of fine particles along lath boundaries led to the appearance of almost continuous chains of Laves phase particles at some of these boundaries. No strain-induced coarsening was detected (Figs. 9c, 10a–d). The dimensions of the Laves phase particles were nearly the same after long-term aging and short-term creep (Table 1).

Insignificant additional precipitation of the $M_{23}C_6$ carbides could be observed. In general, the dimensions of the $M_{23}C_6$ carbides remained nearly unchanged for short-term conditions (Figs. 9c, 10a–d; Table 1). At an applied stress of 140 MPa, weak evidence for strain-induced coarsening of $M_{23}C_6$ carbides appeared (Table 1). The size of these carbides remained ~100 nm up to rupture times of ~5000 h. The Thermo-Calc calculation predicted the existence of a unified (V,Nb)N nitride with a very low C content [45], whereas thermodynamically unstable separation of M(C,N) carbonitrides to Nb-rich and V-rich particles remained during creep condition. The dispersion of M(C,N) carbonitrides changed insignificantly (Fig. 9c).

Long-term creep microstructures

Transformation of the TMLS to a subgrain structure occurred during long-term creep conditions in the same manner as during long-term aging, but a portion of the subgrain structure was significantly greater than after long-term aging (Fig. 10e–f). In contrast with steels containing less W [7, 9–11], this evolution was not followed by extensive subgrain coarsening (Fig. 9a; Table 1). The subgrain size increased insignificantly from 0.6 to 0.8 μm. Only a twofold difference in the lattice dislocation density between the grip and gage sections was observed at 100 MPa. It was obvious that the TMLS exhibited an increased stability during long-term creep conditions. This stability was provided by the dispersion of $M_{23}C_6$ carbides, because extensive coarsening of the Laves phase particles occurs during long-term creep
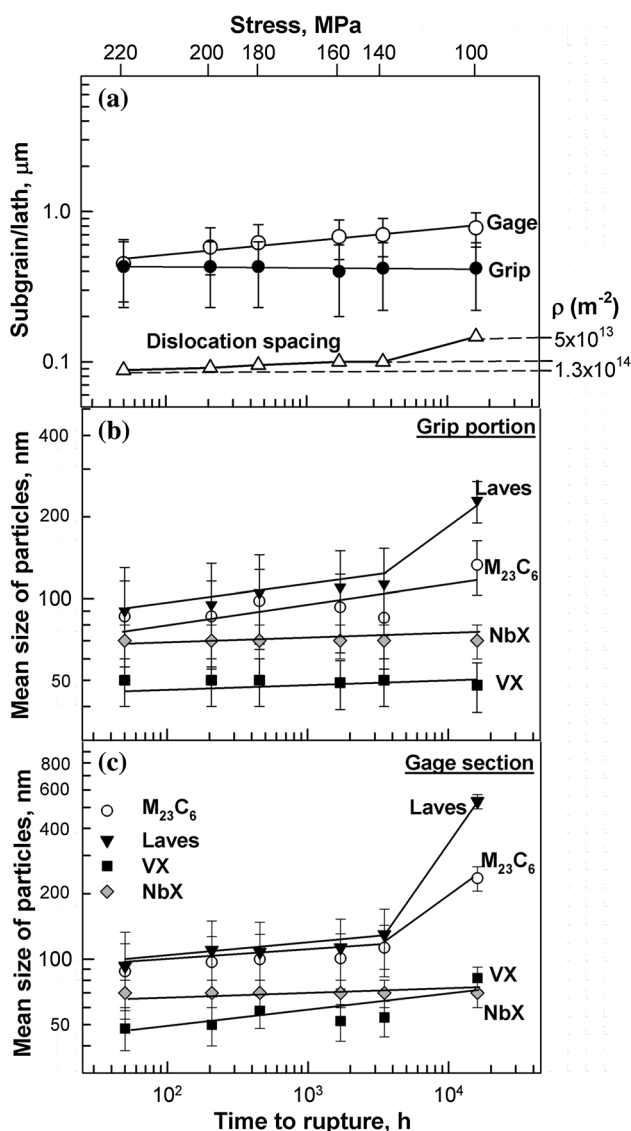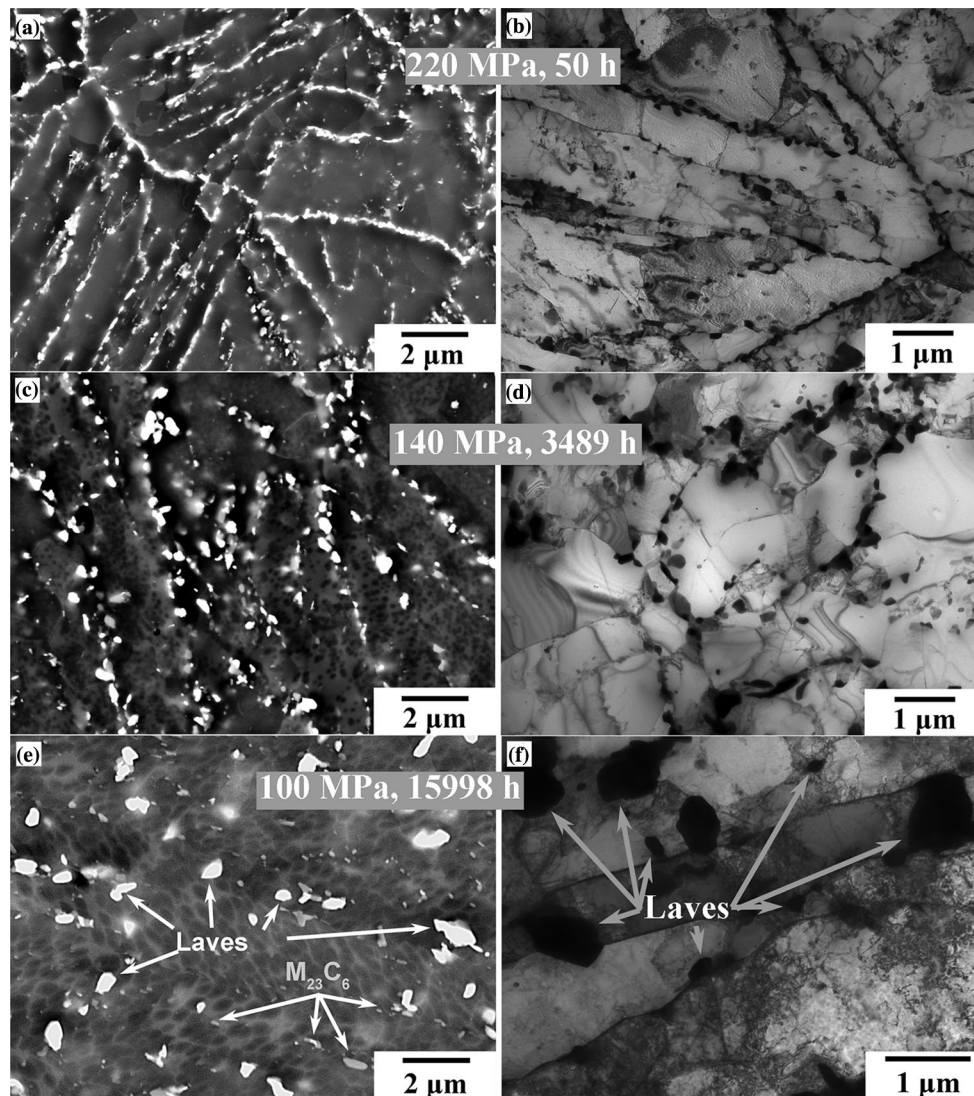
Figure 10 Microstructure of the steel in the gage sections of the specimens after short-term and long-term creep tests at 650 °C and stresses of **a**, **b** 220 MPa (50 h), **c**, **d** 140 MPa (3489 h), and **e**, **f** 100 MPa (15,998 h).

conditions (Figs. 9c, 10e–f; Table 1). The average size of the Laves phase achieved ∼550 nm after a creep test at 100 MPa (rupture time of ∼1.6×10^4 h) due to the rapid strain-induced growth. Distinct strain-induced coarsening of the $M_{23}C_6$ carbides appeared after creep at an applied stress <140 MPa (life time is ∼3.5×10^3 h), and the size of these carbides was >200 nm (Figs. 9c, 10e–f).

No strain-induced coarsening of the Nb-rich M(C,N) occurred during long-term creep conditions (Table 1). In contrast, at an applied stress of 100 MPa, strain-induced coarsening resulted in a +60% increase in the average size of the V-rich M(C,N) particles compared with long-term aging

(Fig. 9b–c; Table 1). In some V-rich carbonitride particles, the portion of Cr exceeded 30 at.% and, therefore, the Z-phase (CrVN nitride) appeared [24]. However, the dimensions of the Z-phase and the V-rich M(C,N) carbonitrides were ∼50 nm, and the portion of Z-phase among all the V-rich carbonitrides was less than 5%. More details of the formation of Z-phase in steel studied were reported in a previous work [53]. Therefore, the formation of the Z-phase was unimportant for the creep resistance of the 9Cr3W steel. In general, long-term creep leads to insignificant changes in the distribution of M(C,N) carbonitrides even at an applied stress of 100 MPa.

Discussion

Increased W content and creep strength breakdown

Inspection of the experimental data showed that the 9Cr3W steel exhibited a well-defined creep strength breakdown that had no well-defined relation with the formation of the Z-phase [24–26] or static recovery [15], because no significant evolution of the dispersion of the M(C,N) carbonitrides under any creep condition and no transformation of a major portion of the lath structure to a subgrain structure occurred during long-term aging. Increasing the W content from 2 to 3 wt% suppresses these processes [7, 9]. The difference in microstructures evolved after creep up to rupture correlates with distinct difference in tertiary creep behavior (Figs. 4a, c, 5, 6) and has no sense to inflection point for creep strength versus rupture time dependence (Fig. 2). The onset of the creep strength breakdown almost matches the complete depletion of the excess W from the solid solution. It is worth noting that the 3 wt% W addition is the most effective in decreasing the off-set strain, and this positive effect was retained after depleting this element and Mo from the solid solution. It is obvious that the precipitation of the fine Laves phase particles at lath boundaries provides this positive effect [27, 29, 42], stabilizing the TMLS and preventing the knitting reaction between the lattice dislocations and the sessile dislocations that compose the lath boundaries.

Effect of applied stress on the Zener drag pressure

The boundary Laves phase particles, $M_{23}C_6$ carbides, and matrix M(C,N) carbonitrides are known to exert different Zener drag forces. The Zener pinning force exerted by the M(C,N) carbonitrides can be evaluated as [7, 9, 10, 22]:

$$P_Z = \frac{3\gamma F_V}{d}, \tag{5}$$

where γ is the boundary surface energy per unit area (0.153 J/m^2), F_v is the volume fraction of the particles calculated using Thermo-Calc, and d is the mean size of particles, m.

The Zener drag pressure exerted by the boundary particles of the $M_{23}C_6$ and Laves phases can be estimated as [7, 9, 10, 22]:

$$P_B = \frac{\gamma F_{vB} D}{d^2}, \tag{6}$$

where D is the subgrain size/lath width in μm, and F_{vB} is the fraction of the particles located at the boundaries. The pinning pressures were calculated separately for the $M_{23}C_6$ carbides and the Laves phase:

$$P_B = \frac{\gamma F_{vB} D_0}{d_0^2} \cdot \frac{\beta_i}{\beta_0}, \tag{7}$$

where β_0 and β_i are the densities of the $M_{23}C_6$ carbides or the Laves phase particles that were located along boundaries for the initial state and for each applied stress. The procedure for calculation of the Zener drag pressure for different types of particles was considered in previous works [7, 9] in detail.

The effect of the applied stress on the Zener drag pressures by three types of precipitates is shown in Fig. 11. It is seen that M(C,N) carbonitrides give an insignificant contribution to the overall pinning pressure for almost all conditions except at an applied stress of 100 MPa at which P_Z and P_B force exerted by the Laves phase particles become nearly equal. The main feature of the present steel is the fact that the greatest Zener drag was exerted by the Laves
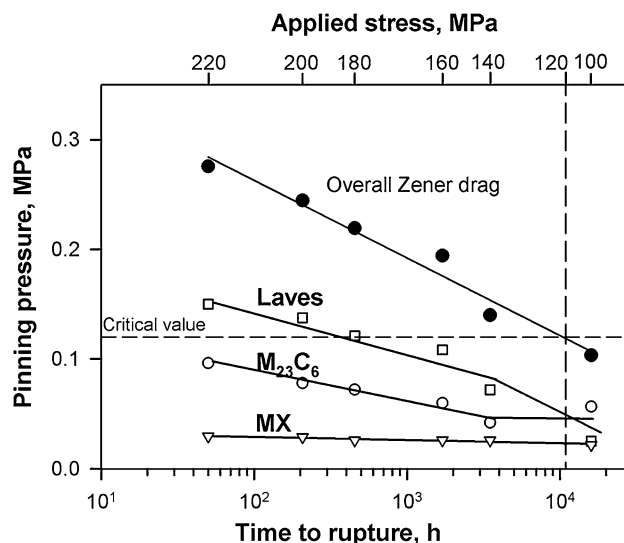

Figure 11 Change in the pinning pressures from the $M_{23}C_6$ carbides, the Laves phase, and the MX carbonitrides in the gage section on the grain and lath boundaries of the steel during creep tests at 650 °C under stresses of 100–220 MPa. The critical value corresponds to the pinning pressure, which is the pressure at which the transformation of TMLS into subgrain structure occurs and is 0.12 MPa based on previous investigations [7].

phase particles at applied stresses greater than 100 MPa, and the $M_{23}C_6$ carbides gave the main contribution to the overall Zener drag force only at an applied stress of 100 MPa. Overall, the Zener drag was great enough at all creep conditions to suppress boundary migration. At applied stresses less than 120 MPa, the overall pinning pressure became equal or less than the critical value of 0.12 MPa, at which the lath structure transformed to a subgrain structure [7]. Therefore, at applied stress ≤120 MPa, the degradation of the Zener drag force below the critical value [7] corresponds to the transition to long-term creep associated with increased rate of acceleration of tertiary creep. However, even at an applied stress of 100 MPa, the overall Zener drag force was able to provide no onset of the extensive subgrain coarsening [7]. As a result, the blocks delimited by the boundaries decorated by the $M_{23}C_6$ and Laves phase particles retain stability during long-term creep, whereas a major part of laths within these blocks transformed to subgrains. Therefore, the transition from short-term creep to long-term creep in the 9Cr3W steel correlates with the strain-induced coarsening of the $M_{23}C_6$ carbides and the Laves phase particles, and leads to transformation of a major part of the lath structure to a subgrain structure and to a remarkable decrease in the lattice dislocation density due to the knitting reaction providing the transformation of lath boundaries to subgrain boundaries followed by their migration.

Role of strain-induced coarsening of boundary particles in creep resistance

In the 9Cr–3Cr–3W steel, the role of high densely distributed and fine particles of Laves phase precipitated at lath boundaries in impeding the knitting reaction between free dislocations and the lath boundaries and exerting Zener forces on the low-angle boundaries is the same as the role of the $M_{23}C_6$ carbides [6, 7, 9, 10, 54]. However, resistance of the Laves phase particles to coarsening is significantly lower than one of the $M_{23}C_6$ carbides, and transition to long-term creep correlates with the onset of extensive coarsening of these particles [29] which leads to the dissolution of the fine particles of Laves phase precipitated at lath boundaries in accordance with well-known Gibbs–Thomson schema [55].

Strain-induced coarsening of $M_{23}C_6$ carbides during creep in high-Cr martensitic steels has been reported in several studies [7, 16, 56, 57]. K. Maruyama et al. showed [56] that the transition to long-term creep was attributed to the coarsening of these carbides in grip sections and to the strain-induced coarsening of these carbides under steady-state and tertiary creep. The 1 wt% W additives highly accelerate the strain-induced coarsening of Laves phase under long-term creep [7]. At an applied stress >120 MPa, under the short-term creep, no pronounced coarsening of these particles takes place in the grip and gage sections of creep specimens. In the long-term creep region, the onset of the tertiary creep stage even at a low strain correlates with the strain-induced coarsening of the $M_{23}C_6$ carbides and the Laves phase particles and a loss of the pinning pressure from these particles.

Abe suggested that precipitation of the Laves phase particles may provide dispersion strengthening [42]. The mechanism of this strengthening is not obvious if a dislocation glides across a lath and does not cross the lath boundaries. A mean dislocation path is equal to the lath thickness. However, it was recently shown by direct TEM observations [19] that dislocation glide occurs along a lath. This glide occurs slowly bowing out because both ends of these dislocations are connected to the mutually opposite lath boundaries. Sessile dislocations that compose the lath boundaries exert a high pinning stress, which is inversely proportional to the lath thickness. Precipitation of the Laves phase particles at the lath boundaries further increases this pinning stress. Climb of dislocation segments is necessary to overcome the boundary $M_{23}C_6$ carbides and Laves phase particles. This is why the depletion of W and Mo from solid solution has a minor effect on the minimum creep rate. The facilitation of general dislocation climb is partially compensated by the pinning stress exerted by the lath boundary particles. In addition, these particles hinder the knitting reaction because local dislocation climb is necessary to bypass these particles, i.e., the role of W and Mo as pinning agents for the knitting reaction as substitutional solutes and in the form of lath boundary Laves phase particles is the same. As a result, the dislocation density is high enough except for the case of creep to rupture when subject to an applied stress of 100 MPa. Strain-induced dissolution of the fine $M_{23}C_6$ carbides and the Laves phase particles at the lath boundaries promotes the knitting reaction, decreases the pinning stress for the dislocation glide, and facilitates

coarsening of the laths and their transformation to subgrains. In the 9Cr3W steel, the transition from short-term creep to long-term creep is primarily attributed to this process.

of the strain-induced particle coarsening on the creep resistance was attributed to the dissolution of the fine Laves phase particles located at the lath boundaries.

Conclusions

1. The 0.1C–9Cr–3Co–3W–0.5Mo–VNbBN martensitic steel exhibited a creep strength breakdown as a sudden drop in the rupture time at 650 °C under an applied stress of 160 MPa. However, transition from short-term creep to long-term creep was characterized by the deviation from the linear dependence of the Monkman–Grant relationship and an increased value of the creep rate by strain in the acceleration region (dln $\dot{\varepsilon}_r/\mathrm{d}\varepsilon$) for low applied stresses and appeared at 120 MPa. No effect of these transitions on the power law relationship between the steady-state creep rate and the applied stress was found. This unique creep behavior is associated with strain-induced precipitation of fine particles of Laves phase at lath boundaries.

2. The TMLS remains nearly unchanged during long-term aging up to $\sim 1.6 \times 10^4$ h and short-term creep due to a very high Zener drag force exerted by the Laves phase particles and the $M_{23}C_6$ carbides. No strain-induced coarsening of these particles and M(C,N) carbonitrides occurred during short-term creep conditions, and coarsening of these particles during long-term aging and short-term creep was insignificant.

3. Creep strength breakdown at an applied stress of 160 MPa correlated with a depletion of excess W from the solid solution after 2000 h of long-term aging, and no evidence of any correlation between the creep strength breakdown appearance and the formation of the Z-phase particles was found. Transition from short-term creep to long-term creep associated with increased rate of acceleration of tertiary creep at an applied stress of 120 MPa was accompanied by the onset of strain-induced coarsening of the Laves phase particles and the $M_{23}C_6$ carbides, which facilitated the partial transformation of the TMLS. However, the Zener drag force exerted by the boundary particles remained high enough to suppress subgrain coarsening. The negative effect

Compliance with ethical standards

Conflict of interest   The authors declare that they have no conflict of interest.

References

[1] Abe F, Kern TU, Viswanathan R (2008) Creep resistant steels. Woodhead Publishing in Materials, Cambridge

[2] Kaybyshev RO, Skorobogatykh VN, Shchenkova IA (2010) New martensitic steels for fossil power plant: creep resistance. Phys Met Metallogr 109:186–200

[3] Kitahara H, Ueji R, Tsuji N, Minamino Y (2006) Crystallographic features of lath martensite in low-carbon steel. Acta Mater 54:1279–1288

[4] Ghassemi-Armaki H, Chen R, Maruyama K, Igarashi M (2010) Premature creep failure in strength enhanced high Cr ferritic steels caused by static recovery of tempered martensite lath structures. Mater Sci Eng A 527:6581–6588

[5] Abe F (2009) Analysis of creep rates of tempered martensitic 9%Cr steel based on microstructure evolution. Mater Sci Eng A 510–511:64–69

[6] Kostka A, Tak K-G, Hellmig RJ, Estrin Y, Eggeler G (2007) On the contribution of carbides and micrograin boundaries to the creep strength of tempered martensite ferritic steels. Acta Mater 55:539–550

[7] Fedoseeva A, Dudova N, Kaibyshev R (2016) Creep strength break down and microstructure evolution in a 3%Co modified P92 steel. Mater Sci Eng A 654:1–12

[8] Taneike M, Sawada K, Abe F (2004) Effect of carbon concentration on precipitation behavior of $M_{23}C_6$ carbides and MX carbonitrides in martensitic 9Cr steel during heat treatment. Metall Mater Trans A 35:1255–1261

[9] Dudova N, Plotnikova A, Molodov D, Belyakov A, Kaibyshev R (2012) Structural changes of tempered martensitic 9%Cr–2%W–3%Co steel during creep at 650°C. Mater Sci Eng A 534:632–639

[10] Dudko V, Belyakov A, Molodov D, Kaibyshev R (2013) Microstructure evolution and pinning of boundaries by precipitates in a 9pctCr heat resistant steel during creep. Metall Mater Trans A 44:162–172

[11] Kipelova A, Kaibyshev R, Belyakov A, Molodov D (2011) Microstructure evolution in a 3%Co modified P911 heat resistant steel under tempering and creep conditions. Mater Sci Eng A 528:1280–1286

[12] Aghajani A, Somsen Ch, Eggeler G (2009) On the effect of long-term creep on the microstructure of a 12% chromium tempered martensite ferritic steel. Acta Mater 57:5093–5106

[13] Abe F (2015) Creep behavior, deformation mechanisms and creep life of mod. 9Cr-1Mo steel. Metall Mater Trans A 46:5610–5625

[14] Ghassemi-Armaki H, Chen R, Maruyama K, Igarashi M (2011) Creep behavior and degradation of subgrain structures pinned by nanoscale precipitates in strength-enhanced 5 to 12 Pct Cr ferritic steels. Metall Mater Trans A 42:3084–3094

[15] Ghassemi-Armaki H, Chen R, Maruyama K, Igarashi M (2013) Contribution of recovery mechanisms of microstructure during long-term creep of Gr.91 steels. J Nucl Mater 433:23–29

[16] Eggeler G (1989) The effect of long-term creep on particle coarsening in tempered martensite ferritic steels. Acta Metall 37:3225–3234

[17] Fournier B, Sauzay M, Pineau A (2011) Micromechanical model of the high temperature cyclic behavior of 9–12%Cr martensitic steels. Int J Plast 27:1803–1816

[18] Sauzay M (2009) Modelling of the evolution of micro-grain misorientations during creep of tempered martensite ferritic steels. Mater Sci Eng A 510–511:74–80

[19] Mitsuhara M, Yamasaki S, Miake M, Nakashima H, Nishida M, Kusumoto J, Kanaya A (2016) Creep strengthening by lath boundaries in 9Cr ferritic heat-resistant steel. Philos Mag Lett 96:76–83

[20] Magnusson H, Sandstrom R (2007) Creep strain modeling of 9 to 12 Pct Cr steels based on microstructure evolution. Metall Mater Trans A 38:2033–2039

[21] Dudko VA, Belyakov AN, Kaibyshev RO (2015) Sources of high creep resistance of modern high-chromium martensitic steels. Dokl Phys Chem 464:191–193

[22] Humphreys FJ, Hatherly M (2004) Recrystallization, related annealing phenomena, 2nd edn. Elsevier, Oxford

[23] Dudko V, Belyakov A, Kaibyshev R (2016) Origin of threshold stresses in a P92-type steel. Trans Indian Inst Met 69:223–227

[24] Cipolla L, Danielsen HK, Venditti D, Di Nunzio PE, Hald J, Somers MAJ (2010) Conversion of MX nitrides to Z-phase in a martensitic 12% Cr steel. Acta Mater 58:669–679

[25] Hald J (2016) Prospects for martensitic 12% Cr steels for advanced steam power plants. Trans Indian Inst Met 69:183–188

[26] Rojas D, Garcia J, Prata O, Sauthoff G, Kaysser-Pyzalla AR (2011) 9%Cr heat resistant steels: alloy design, microstructure evolution and creep response at 650°C. Mater Sci Eng A 528:5164–5176

[27] Prat O, Garcia J, Rojas D, Sauthoff G, Inden G (2013) The role of Laves phase on microstructure evolution and creep strength of novel 9%Cr heat resistant steels. Intermetallics 32:362–372

[28] Rojas D, Garciab J, Prat O, Agudo L, Carrasco C, Sauthoff G, Kaysser-Pyzalla AR (2011) Effect of processing parameters on the evolution of dislocation density and sub-grain size of a 12%Cr heat resistant steel during creep at 650°C. Mater Sci Eng A 528:1372–1381

[29] Prat O, Garcia J, Rojas D, Carrasco C, Inden G (2010) Investigations on the growth kinetics of Laves phase precipitates in 12% Cr creep-resistant steels: experimental and DICTRA calculations. Acta Mater 58:6142–6153

[30] Helis L, Toda Y, Hara T, Miyazaki H, Abe F (2009) Effect of cobalt on the microstructure of tempered martensitic 9Cr steel for ultra-supercritical power plants. Mater Sci Eng A 510–511:88–94

[31] Kipelova A, Odnobokova M, Belyakov A, Kaibyshev R (2013) Effect of Co on creep behavior of a P911 steel. Metall Mater Trans A 44:577–583

[32] Abe F, Nakazawa Sh (1991) The effect of tungsten on creep behavior of tempered martensitic 9Cr steels. Metall Trans A 23:3025–3034

[33] Vanaja J, Laha K, Mathew MD (2014) Effect of tungsten on primary creep deformation and minimum creep rate of reduced activation ferritic-martensitic steel. Metall Mater Trans A 45:5076–5084

[34] Vanaja J, Laha K (2016) Assessment of tungsten content on tertiary creep deformation behavior of reduced activation ferritic–martensitic steel. Metall Mater Trans A 46:4669–4679

[35] Sawada K, Takeda M, Maruyama K, Ishii R, Yamada M, Nagae Y, Komine R (1999) Effect of W on recovery of lath structure during creep of high chromium martensitic steels. Mater Sci Eng A 267:19–25

[36] Hong SG, Lee WB, Park CG (2001) The effect of tungsten addition on the microstructural stability of 9Cr-Mo steel. J Nucl Mater 288:202–207

[37] Isik MI, Kostka A, Yardley VA, Pradeep KG, Duarte MJ, Choi PP, Raabe D, Eggeler G (2015) The nucleation of Mo-rich Laves phase particles adjacent to $M_{23}C_6$ micrograin boundary carbides in 12% Cr tempered martensite ferritic steels. Acta Mater 90:94–104

[38] Fedorova I, Belyakov A, Kozlov P, Skorobogatykh V, Shenkova I, Kaibyshev R (2014) Laves phase precipitates in a low-carbon 9%Cr martensitic steel during aging and creep at 923 K. Mater Sci Eng A 615:153–163

[39] Kipelova A, Belyakov A, Kaibyshev R (2012) Laves phase evolution in a modified P911 heat resistant steel during creep at 923K. Mater Sci Eng A 532:71–77

[40] Zhu S, Yang M, Song XL, Zhang Z, Wang LB, Tang S, Xiang ZD (2014) A few observations on Laves phase precipitation in relation to its effects on creep rupture strength of ferritic steels based on Fe–9Cr (wt%) alloys at 650 °C. Mater Sci Eng A 619:47–56

[41] Li Q (2006) Precipitation of Fe_2W Laves phase and modeling of its direct influence on the strength of a 12Cr-2 W steel. Metall Mater Trans A 37:89–97

[42] Abe F (2005) Effect of fine precipitation and subsequent coarsening of Fe_2W Laves phase on the creep deformation behavior of tempered martensitic 9Cr-W steels. Metall Mater Trans A 36:321–332

[43] Kimura K, Sawada K, Kushima H, Kubo K (2008) Effect of stress on creep deformation property of ASME Grade P92/T92 steels. J Mater Res 99:395–401

[44] Hirsch PB, Howie A, Nicholson RB et al (1977) Electron microscopy of thin crystals, 2nd edn. Krieger, New York

[45] Fedoseeva A, Dudova N, Glatzel U, Kaibyshev R (2016) Effect of W on tempering behaviour of a 3%Co modified P92 steel. J Mater Sci 51:9424–9439. doi:10.1007/s10853-016-0188-x

[46] Tabuchi M, Hongo H, Abe F (2014) Creep strength of dissimilar welded joints using high B-9Cr steel for advanced USC boiler. Metall Mater Trans A 45:5068–5075

[47] Liu Y, Tsukamoto S, Sawada K, Tabuchi M, Abe F (2015) Precipitation behavior in the heat-affected zone of boron-added 9Cr-3 W-3Co steel during post-weld heat treatment and creep deformation. Metall Mater Trans A 46:1843–1854

[48] Kaibyshev R, Mishnev R, Tkachev E, Dudova N (2016) Effect of Ni and Mn on the creep behavior of 9-10%Cr steels with low N and high B. Trans Indian Inst Met 69:203–210

[49] Cadek J (1994) Creep in metallic materials. Academia, Prague

[50] Kassner ME, Pérez-Prado MT (2004) Fundamentals of creep in metals and alloys, 1st edn. Elsevier, New York

[51] Monkman FC, Grant NJ (1956) Relationship between rupture life and minimum creep rate in creep-rupture tests. Proc ASTM 56:593–620

[52] Dudova N, Kaibyshev R (2011) On the precipitation sequence in a 10%Cr steel under tempering. ISIJ Int 51:826–831

[53] Fedoseeva A, Dudova N, Kaibyshev R (2016) Effect of tungsten on a dispersion of M(C, N) carbonitrides in 9% Cr steels under creep conditions. Trans Indian Inst Met 69(2):211–215

[54] Mishnev R, Dudova N, Fedoseeva A, Kaibyshev R (2016) Microstructural aspects of superior creep resistance of a 10%Cr martensitic steel. Mater Sci Eng A 678:178–189

[55] Porter DA, Esterling KE, Sherif M (2009) Phase transformation in metals and alloys, 3rd edn. CRS Press, Boca Raton

[56] Hattestrand A, Andren HO (2001) Influence of strain on precipitation reactions during creep of an advanced 9% chromium steel. Acta Mater 49:2123–2128

[57] Ghassemi-Armaki H, Chen R, Kano S, Maruyama K, Hasegawa Y, Igarashi M (2012) Strain-induced coarsening of nanoscale precipitates in strength enhanced high Cr ferritic steels. Mater Sci Eng A 532:373–380